Selected for a Viewpoint in *Physics*

PHYSICAL REVIEW B **83**, 035321 (2011)

Demonstration of molecular beam epitaxy and a semiconducting band structure for I-Mn-V compounds

T. Jungwirth,[1,2] V. Novák,[1] X. Martí,[3] M. Cukr,[1] F. Máca,[4] A. B. Shick,[4] J. Mašek,[4] P. Horodyská,[3] P. Němec,[3] V. Holý,[3]
J. Zemek,[1] P. Kužel,[4] I. Němec,[5] B. L. Gallagher,[2] R. P. Campion,[2] C. T. Foxon,[2] and J. Wunderlich[1,6]
[1]*Institute of Physics ASCR, v.v.i., Cukrovarnická 10, 162 53 Praha 6, Czech Republic*
[2]*School of Physics and Astronomy, University of Nottingham, Nottingham NG7 2RD, United Kingdom*
[3]*Faculty of Mathematics and Physics, Charles University in Prague, Ke Karlovu 3, 121 16 Prague 2, Czech Republic*
[4]*Institute of Physics ASCR, v.v.i., Na Slovance 2, 182 21 Praha 8, Czech Republic*
[5]*Faculty of Science, Charles University in Prague, Hlavova 2030, 128 40 Prague 2, Czech Republic*
[6]*Hitachi Cambridge Laboratory, Cambridge CB3 0HE, United Kingdom*

(Received 29 November 2010; published 24 January 2011)

Our *ab initio* theory calculations predict a semiconducting band structure of I-Mn-V compounds. We demonstrate on LiMnAs that high-quality materials with group-I alkali metals in the crystal structure can be grown by molecular beam epitaxy. Optical measurements on the LiMnAs epilayers are consistent with the theoretical electronic structure. Our calculations also reproduce earlier reports of high antiferromagnetic ordering temperature and predict large, spin-orbit-coupling-induced magnetic anisotropy effects. We propose a strategy for employing antiferromagnetic semiconductors in high-temperature semiconductor spintronics.

DOI: 10.1103/PhysRevB.83.035321 PACS number(s): 78.30.Fs, 71.22.+i, 75.50.Pp, 81.15.Hi

I. INTRODUCTION

Current spintronic applications are based on ferromagnetically (FM) ordered spins of transition metals such as Ni, Co, Fe, and their alloys.[1] These material systems have provided the strong magnetoresistive effects essential to the development of commercial spintronics. However, there are fundamental physical limitations for FM metal materials that may make them impractical to realize the full potential of spintronics. Metals are unsuitable for transistor and information processing applications, for optoelectronics, and the large magnetic stray fields produced by these materials also make them unfavorable for high-density integration. A considerable effort has been directed toward overcoming these limitations by developing FM semiconductor materials based on conventional semiconductor hosts. (III,Mn)V compounds are among the most extensively explored examples of these systems.[2] They do not allow for the high-temperature operation but they are ideal test bed materials for exploring new spintronic concepts.

The inspiration for the work presented in this paper comes from discoveries of relativistic magnetic and magnetotransport anisotropy effects in (III,Mn)V nanodevices,[2,3] which have the desired large magnitudes and whose common characteristics is that they are an even function of the microscopic magnetic moment vector. The concept, whose generic validity has been recently confirmed in transition-metal FMs[4–6] and antiferromagnets (AFMs),[7,8] paves the way to spintronics in a wide range of systems, including semiconducting materials with antiferromagnetically coupled moments. This has inspired our search for antiferromagnetic semiconductors suitable for high-temperature spintronics. While the theoretical work presented in this paper, which further elaborates on the AFM spintronics concept, has implications for a broad range of candidate AFM semiconductors, we focus here on magnetic counterparts of the most common semiconductor compounds.

The most common compound semiconductors are derived from silicon by applying the “proton transfer” rule.[9] The first branch of these compounds considers proton transfer from one to the other atom in the silicon primitive cell. The resulting III–V and II–VI semiconductors are artificial materials that became particularly popular with the development of modern epitaxial growth techniques with atomic layer resolution. The branch hosts the prototype FM and AFM semiconductors such as the Mn-VI compounds. The magnetic transition temperatures, however, do not safely exceed room temperature in any of the known magnetic II–VI or III–V compounds.

The second branch of immediate silicon relatives comprises I–III–IV and I–II–V compounds in which a proton is transferred into an empty interstitial space in the primitive cell. They were recognized before III–V compounds in the early 1930’s,[10] shortly after the introduction of the concept of semiconductors. The crystal structure of several known examples of these artificial alkali-metal compounds is similar to the other silicon relatives, as illustrated in Fig. 1. From the few reports available in the literature we can also infer standard semiconducting optical and electrical characteristics. LiZnAs, e.g., is a direct-gap semiconductor with a band gap of 1.6 eV similar to GaAs, it shows photoluminescence, and the mobilities of chemically synthesized bulk samples are comparable to the bulk GaAs counterparts.[11]

A remarkable feature of the second branch emerges from reports on neutron-diffraction measurements in I-Mn-V compounds. These experiments identified AFM coupling in the Mn planes persisting to very high temperatures and a weaker interlayer magnetic coupling that still persists in most of the I-Mn-V compounds above 400 K.[12–14] However, to the best of our knowledge, no experimental or theoretical report published to date has considered I-Mn-V compounds to be semiconductors, and no report has been published on epilayer growth of I-Mn-V’s (or of any other compound with group-I alkali metals in the crystal structure).

Before we proceed to the discussion of our experimental and theoretical results, we make a few additional general remarks on the combination of magnetic and semiconducting properties in one physical material. In Fig. 2(a) we illustrate that a strong

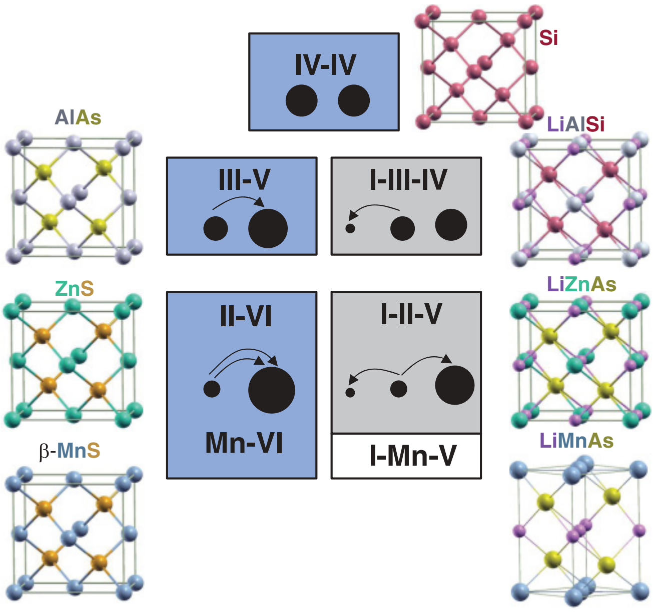

FIG. 1. (Color online) Two branches of the closest relatives of silicon emerging from the "proton transfer" rule. The left-hand branch is obtained by imagining one or two proton transfer from the first to the second atom of the primitive cell; the right-hand branch assumes that one proton is transferred into an empty interstitial space in the lattice. Common representatives of these basic semiconductor groups have similar crystal structures as depicted in the figure. Owing to its isovalent nature, Mn naturally extends the elements from the group-II zinc column. Prior to this work, epitaxial growth of the right-hand branch compounds have not been reported and I-Mn-V compounds have not been considered as candidate semiconductors.

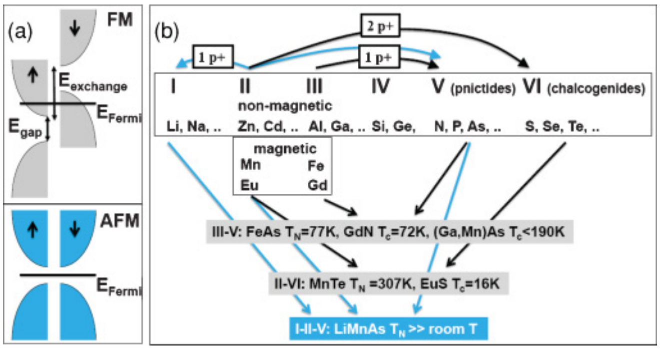

FIG. 2. (Color online) (a) Illustration of the competition between the band gap and the FM exchange splitting, which results in the Fermi energy inside the band, i.e., metal character, for large enough exchange splittings. The absence of this competition in AFMs makes strong AFM semiconductors more likely to occur than strong FM semiconductors. (b) Illustration of the survey of magnetic semiconductor counterparts to conventional semiconductors with eight valence electrons per primitive cell. Consistent with (a), most of the magnetic semiconductors are AFMs and the more rare FM semiconductors are found primarily among compounds with more localized (less hybridized) f-electron magnetic elements and lighter anions (wider band gaps). Magnetic transition temperatures safely above room temperature are found in the compounds containing the group-I element, and I-Mn-V's are the simplest representatives of this class of materials.

AFM ground state is, from the basic physics perspective, much more compatible with a gapped, semiconductorlike band structure than a strong FM state. In the FM case, the gap competes with the exchange spin splitting of the bands that at strong FM coupling turns the system into a metal. In AFMs, this competition is missing, and indeed a large majority of magnetic semiconductors order antiferromagnetically.

Because there is no direct realization of a magnetic semiconductor within the group-IV crystals, we need to proceed to compounds [see Fig. 2(b)]. Here FeAs is an example of an AFM semiconductor from the III–V family. As implied by Fig. 2(a), the less frequent FM semiconductors have a better chance to occur among the more localized (less hybridized) f-electron magnetic elements and the lighter anions (wider gap). The GdN FM semiconductor belongs to this group of materials. Transition temperatures of all the III–V magnetic semiconductors are below room temperature and the non-half-filled shell of the magnetic element is one of the reasons for weaker magnetic interactions. Indeed, (Ga,Mn)As already suggests that using Mn with the half-filled magnetic shell, i.e., highest moment among the $3d$ magnetic elements, has a favorable effect on the strength of magnetic coupling. [Recall that the (Ga,Mn)As random alloy is not an intrinsic but rather a heavily doped degenerate semiconductor because Mn_{Ga} is not an isovalent impurity.] Consistent with this trend, there are a number of Mn-chalcogenide AFM semiconductors and there are also several FMs among the f-electron and lighter anion II–VI compounds. Still, the transition temperatures of II–VI magnetic semiconductors do not safely exceed room temperature. Here the larger anions and more ionic bonds compared to the III–V's result in larger lattice parameters, which softens the magnetic interactions. The I-Mn-V compounds discussed in this paper combine the favorable tighter lattice arrangement of the group-V pnictides and the large magnetic moment on Mn, consistent with the observed high Néel temperatures in these materials.[12–14]

The experimental investigation of epitaxial growth and characterization of LiMnAs layers is presented in Sec. II. In Sec. III we present full-potential *ab initio* density-functional calculations of the electronic structure, optical properties, and relativistic magnetic anisotropy effects in LiMnAs (and several other I-Mn-V compounds). A brief summary of our work is given in Sec. IV.

II. GROWTH AND CHARACTERIZATION OF LiMnAs EPILAYERS

For the epitaxial growth of LiMnAs, we used the III–V InAs substrate because it is commonly available and because the crystallographically equivalent As planes in InAs and in LiMnAs have very similar lattice parameters (4.283 Å in InAs versus 4.267 Å in LiMnAs). The comparison between the respective crystal structures (see Fig. 1) further implies that, starting from the common As plane, LiMnAs should grow epitaxially under a small tensile strain with its Mn planes rotated by 45° with respect to the counterpart In planes of the substrate. Because MnAs is a metal with a hexagonal crystal structure, we have also prepared reference MnAs samples deposited on InAs to highlight the striking consequences of

Li incorporation during the growth on both the crystal and electronic band structures of the material.

For this work we have grown a series of LiMnAs-InAs wafers in a Kryovak molecular beam epitaxy (MBE) system equipped with Li, Mn, and As solid sources. Before the growth, the surface oxide on the InAs substrate was desorbed in the As atmosphere at 450 °C. The LiMnAs films were deposited directly on the substrate at low temperatures (∼150 °C) without growing any preceding buffer layer. The respective cell temperatures were 430 °C (Li), 840 °C (Mn), and 260 °C (As), producing fluxes of the elements at an approximately stoichiometric ratio of 1:1:1. The reproducibility of the growth conditions have been tested over many growth cycles, showing no degradation or apparent damage to the MBE system owing to the presence of large amounts of Li.

The reflection high-energy electron diffraction (RHEED) images were recorded *in situ* during the growth. Within the first few minutes of the growth, a sharp and stable 1×1 RHEED pattern, shown in Fig. 3(a), emerged from the original pattern of the $c(4 \times 4)$ reconstructed surface of the InAs substrate. The LiMnAs RHEED images demonstrate the two-dimensional (2D) growth mode of a high-quality epilayer and confirm the expected in-plane square symmetry of the LiMnAs crystal. The results are in striking contrast to the measurement of the reference MnAs epilayer, shown in Fig. 3(b), deposited on the InAs substrate under the same growth conditions, except for the Li cell remaining closed during the growth. The MnAs sample shows an asymmetric and low epitaxial quality RHEED pattern as a result of the large lattice mismatch of MnAs.

In parallel to the RHEED, which did not show clear oscillations, the growth process of the LiMnAs epilayers was monitored by *in situ* measurements of Fabry-Pérot interference oscillations, shown in Fig. 3(c). In the experiment, the light emitted by the cells in the MBE system, reflected by the growing film, and transmitted outside the chamber through an optical port was recorded by a spectrometer in a spectral range of 870–1400 nm (0.855–1.425 eV). The presence of the Fabry-Pérot oscillations up to a large film thickness is a strong indication of the semiconducting nature of the band structure of LiMnAs. Note that the LiMnAs film thicknesses and the derived growth rate of ∼200 nm/h were obtained by measuring the final thickness profile of the wafers across the edges masked by the sample holder during the growth by the Dektak profiler [see Fig. 3(d)]. The 20% uncertainty in the determination of the LiMnAs film thickness is owing to the surface oxide layer that forms in air and/or owing to the capping layer deposited onto the LiMnAs film to prevent its oxidation. Fabry-Pérot oscillations in the upper part of Fig. 3(c) correspond to the InAs cap and are consistent with its refractive index 3.5. The lower part recorded during the LiMnAs growth yields a smaller refractive index (by a factor of 1.5–2), suggesting that LiMnAs has a larger band gap than InAs.

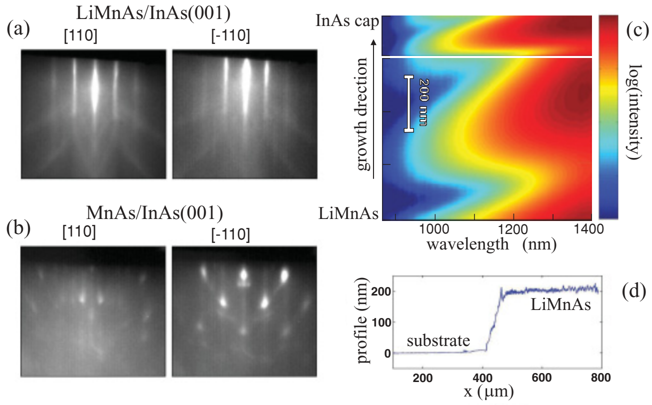

FIG. 3. (Color online) RHEED images (a) of the LiMnAs film and (b) of the MnAs film after 60 min of MBE growth at identical conditions, except for the Li cell closed in case of the MnAs. (c) Fabry-Pérot interference oscillations of the light back-reflected by the growing LiMnAs film on an InAs substrate plotted as a function of the growth time and wavelength of the detected light. The oscillatory interferences are typical of a semiconductor film. (d) Thickness profile of a LiMnAs wafer across the edges masked by the sample holder during the growth. The total growth time of this wafer was 60 min, resulting in ∼200-nm-thick LiMnAs epilayer.

The incorporation of Li and Mn in the grown epilayers was confirmed *ex situ* by a series of sputtering and x-ray photoemission measurements that showed, within the experimental scatter, the expected 1:1 ratio of Li and Mn inside the film. X-ray diffraction experiments presented in Fig. 4 prove that the films are epitaxial. In addition to the InAs substrate peaks, the diffraction curve in Fig. 4(a) shows the full set of (001)-oriented LiMnAs reflections and no traces of other phases or orientations. Note that the peaks are slightly shifted to higher angles with respect to the bulk values (denoted by crosses), in agreement with the expected tensile strain in the LiMnAs epilayer on InAs. In order to investigate the epitaxial relationship, we performed azimuthal scans as a function of the wave vector Q [see Fig. 4(b)]. The data show that the LiMnAs(102) and InAs(131) reflections are separated by an angle $\phi = 26.7^\circ$, which matches the nominal separation in the case of a 45° in-plane rotation of the LiMnAs unit cell with respect to the substrate. Hence, the [110] LiMnAs direction is parallel to the [100] InAs direction, as illustrated in the schematic 3D diagram in Fig. 4(b). Reciprocal space maps shown in Fig. 4(c) evidence the vertical alignment of the substrate and film peak, i.e., the LiMnAs film is an epitaxial single crystal fully strained to the InAs substrate. The upper (black) and lower (red) crosses in the plot denote the expected positions for the substrate and bulk LiMnAs, respectively. Owing to the in-plane tensile strain, the out-of-plane parameter is contracted, leading to the displacement of the LiMnAs(204) reflection toward smaller Q_x values. As a result of this small structural distortion, the unit-cell volume of the LiMnAs epilayer is increased by 0.2%.

Based on the equivalence between the lattice structure of our LiMnAs single-crystal epilayers and of the previously chemically synthesized polycrystalline bulk materials, we expect the same AFM structure of the epilayers. Neutron-diffraction measurements on thin-film epilayers are not routinely available and attempts to perform these magnetic structure experiments on LiMnAs are beyond the scope of this initial work. Instead we performed superconducting quantum interference device (SQUID) measurements of the magnetization, which are shown in Fig. 4(d). The data are consistent with the picture of compensated Mn moments in the

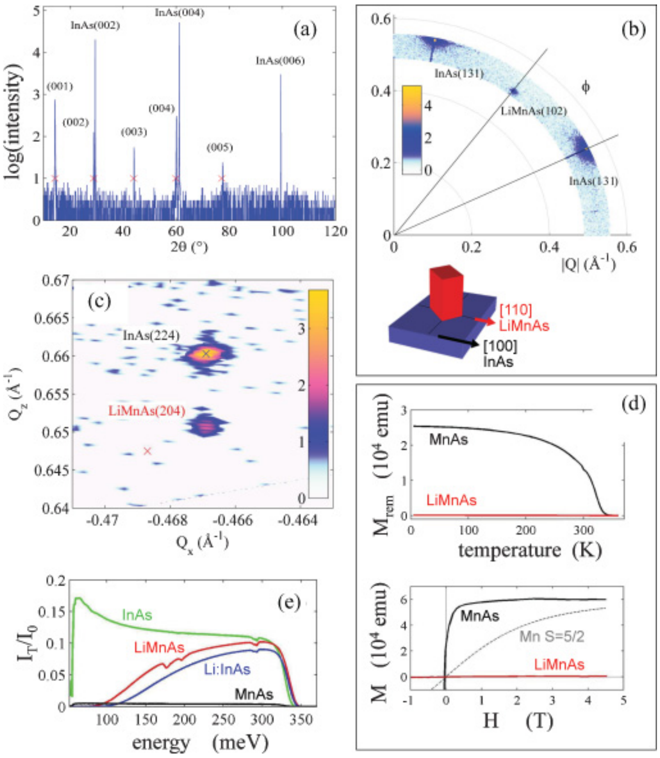

FIG. 4. (Color online) (a) Full set of (001)-oriented LiMnAs x-ray reflections. Bulk values are denoted by crosses. (b) Azimuthal scans as a function of the wave vector Q. The corresponding 45° in-plane rotation of the LiMnAs unit cell with respect to the InAs substrate is illustrated in the inset. (c) Reciprocal space maps evidencing the vertical alignment of the substrate peak and the peak of the strained LiMnAs film. The black and red crosses in the plot denote the expected positions for the substrate and bulk LiMnAs, respectively. (d) Temperature-dependent remanence at 0.2 mT and magnetic-field-dependent magnetization at 4 K of a 200-nm-thick LiMnAs epilayer (red curve) and of the FM MnAs sample (solid black curve) containing the same amount of Mn. For comparison, we also show the theoretical Brillouin function, which describes magnetization at 4 K of an equal number of Mn atoms represented by uncoupled paramagnetic $S = 5/2$ spins in the external magnetic field. (e) Transmissivity of the LiMnAs-InAs sample (red curve) in the near infrared region measured *ex situ* and compared to the MnAs-InAs sample (black curve), to an unprocessed InAs substrate (green curve), and to a Li-doped InAs substrate (blue curve).

AFM LiMnAs. The comparison of the temperature-dependent remanence in LiMnAs and in the reference FM MnAs with the same amount of Mn in the epilayer, as well as the comparison of the low-temperature saturation in LiMnAs, MnAs, and of the theoretical Brillouin function of uncoupled Mn $S = 5/2$ moments, rule out ferromagnetic and paramagnetic behavior of Mn in our LiMnAs epilayers. In agreement with the high Néel temperature of the chemically synthesized bulk materials, we found no signatures of the vicinity of the critical point in the susceptibility in the explored temperature range up to 400 K.

The *ex situ* optical transmission measurements of the LiMnAs grown on InAs are shown in Fig. 4(e). The observed transparency of the wafer (up to the band-gap energy of the 0.5-mm-thick InAs substrate) complements the above *in situ* optical data. The optical transparency of LiMnAs is in striking contrast to the control MnAs sample that, owing to its metallic band structure, is strongly absorbing over the entire studied spectral range, as shown in Fig. 4(e). We note that the enhanced absorption in the LiMnAs-InAs wafer at the low-energy side of the spectrum is owing to free carriers introduced by Li diffused into the InAs substrate during the growth. Interstitial Li acts as a shallow donor in InAs and the resulting *n*-type doping of InAs can be as high as $\sim 10^{18}$ cm^{-3} under our growth conditions. We made these observations based on our control experiment in which the InAs substrate was exposed in the MBE chamber to the Li flux alone. In the resulting InAs:Li we observe again the enhanced low-energy absorption that is correlated with high dc conductivity of the sample. After annealing the Li out of the InAs, the transparency at low energies is recovered and the conductivity drops to the nominal value of the unprocessed substrate.

III. THEORY

We now proceed to the theoretical investigation of the electronic structure of the I-Mn-V compounds. We have performed band-structure calculations of LiMnAs, NaMnAs, and KMnAs by using the full-potential density-functional theory. We found that the AFM state always has lower energy than the FM state. In LiMnAs, the difference in the generalized gradient approximation (GGA) is 34.4 mRy/atom (32.7 mRy/atom in LDA) and, similarly in NaMnAs and KMnAs, the AFM state is lower in energy by 32.9 and 32.5 mRy/atom, respectively. These values, which can be used to estimate the Néel temperature T_N, are larger in the I-Mn-V's than in metal Mn-based alloys whose $T_N \sim 10^3$ K.[15] Our calculations therefore reproduce not only the ground-state AFM structure of the I-Mn-V's but also explain the high T_N observed in neutron-scattering experiments.[12–14] We also

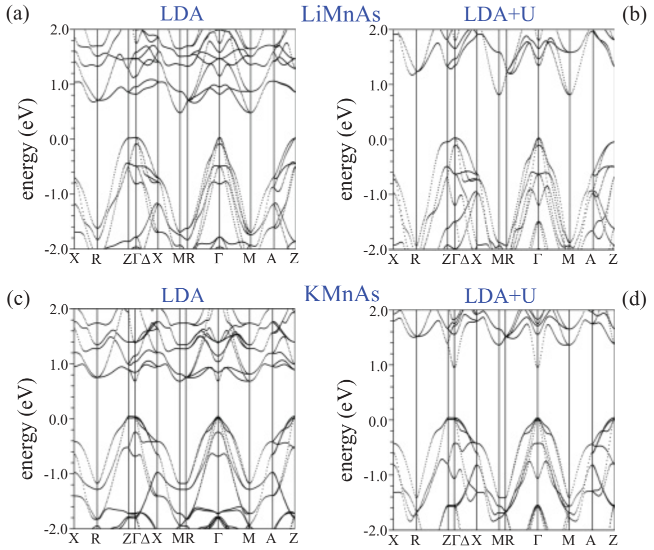

FIG. 5. (Color online) (a) Full-potential LDA calculations of the band dispersions of AFM LiMnAs. Spin-orbit coupling is turned off in this plot for clarity. (b) LDA + U band dispersions of LiMnAs. (c) LDA, (d) LDA + U band dispersions of KMnAs.

remark that our *ab initio* calculations show that the AFM ground state is comparably stable in the intrinsic material and in highly *n*- or *p*-type doped LiMnAs (we considered supercells corresponding to doping as high as $\sim 10^{21}$ cm^{-3}).

All studied I-Mn-V compounds are intrinsic semiconductors for the stoichiometric composition 1:1:1 of the constituent elements; the band dispersions obtained within the local-density approximation without and with correlation corrections (LDA and LDA + U) of LiMnAs and KMnAs are shown in Figs. 5(a)–5(d). Note that the calculated band gaps are likely underestimated by the density-functional theory. Besides the common shortcomings of the LDA, the accurate theoretical determination of the band gap is further complicated by correlation effects on Mn *d* orbitals. The states are, on the one hand, admixed in the top valence-band states and bottom conduction-band states, as shown by the density of states (DOS) plotted in Figs. 6(a) and 6(b), but on the other hand, are still significantly more localized than the *sp* states. Accounting for these effects in LDA + U increases significantly the band gap and suppresses the relative difference between the indirect and direct gaps. In KMnAs, the correlations even change the character of the material from an indirect-gap semiconductor to a direct-gap semiconductor.

The admixture of Mn *d* orbitals in the valence- and conduction-band DOSs and correlations on these states have a significant effect on the dielectric properties of I-Mn-V's. As shown in Fig. 6(c), the increase of the band gap in LiMnAs in the LDA + U and the corresponding shift of the absorption edge in the imaginary part of the dielectric function are correlated with the suppression of the real part of the dielectric function. The large suppression by nearly a factor of 2 is owing partly to the common scaling in semiconductors between the band gap and the refractive index, but, to a large extent, also owing to the optical transitions involving the *d* orbitals. These transitions contribute strongly to the dielectric function, and their shift to higher energies in the LDA + U further reduces the real part of the dielectric function and of the refractive index. The resulting values are consistent with the relatively low refractive index of LiMnAs inferred from the Fabry-Pérot oscillations in Fig. 3(c). Similarly, the significantly larger band gap of LiMnAs compared to InAs is consistent with optical measurements on our LiMnAs-InAs epilayers.

In the concluding paragraphs of this section we discuss a concept of high-temperature AFM semiconductor spintonics. We focus on I-Mn-V AFMs, however, the conclusions of this discussion are generic to a broad range of spin-orbit-coupled AFM semiconductors. The key principle is to utilize relativistic magnetic and magnetotransport anisotropy effects. Our *ab initio* calculations show a sizable magnetocrystalline anisotropy energy (MAE) of ~ 0.6 meV/f.u. in LiMnAs. (This value is 10× larger than in Co.) The MAE is one of the key parameters determining the coupling between a FM and an AFM, which is utilized for pinning the FM via the exchange-bias effect in giant or tunneling magnetoresistance sensor and memory devices.[1] The application of AFM semiconductors to exchange-bias FMs opens an immediate research opportunity for integrating conventional semiconductor functionalities directly in the exchange-biasing AFM layers in common spintronic devices. In the case of LiMnAs, these structures may comprise lattice-matched FM semiconductor (In,Mn)As or conventional transition-metal FMs.

The FM-AFM coupling can be used also for controlling the staggered moment orientation in the AFM by the exchange spring effect induced by rotating moments in the FM.[16] Recently this effect has been demonstrated at $\lesssim 50$ mT applied field and combined with the detection of $>100\%$ AFM tunneling anisotropic magnetoresistance in a NiFe-MnIr-MgO-Pt stack.[8] Our relativistic *ab initio* calculations of the DOS anisotropy shown in Fig. 6(d) illustrate the possibility of similarly strong tunneling magnetotransport anisotropies in AFM semiconductors and, in addition, the possibility to control these effects by doping or electrical gating.

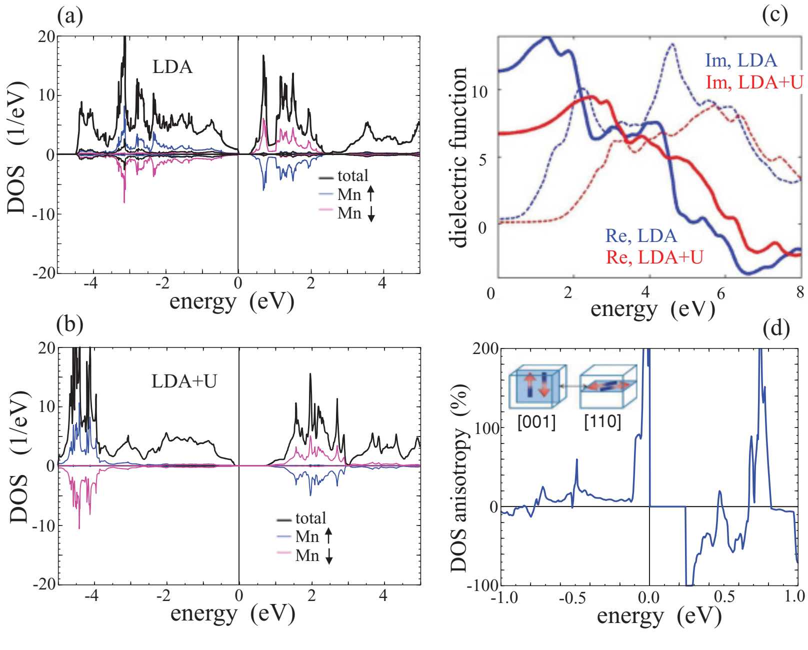

FIG. 6. (Color online) Total and element-resolved DOS of LiMnAs calculated in (a) LDA and (b) LDA + U. (c) Complex dielectric function of LiMnAs in the out-of-plane direction calculated in the LDA and LDA + U. (d) Relativistic full-potential LDA calculations of the anisotropy in the DOS with respect to the staggered moment orientation along the [001] and [110] crystal axes. These anisotropies are order of magnitude larger than in the metal Mn-based AFMs and vary strongly near the valence- and conduction-band edges.

IV. SUMMARY

To summarize, our *ab initio* calculations predict a semiconducting band structure of I-Mn-V compounds, confirm that these materials are strong AFMs, and unveil a strong spin-orbit-coupling character of conduction- and valence-band states favorable for spintronics. In the experimental part of our study, we demonstrate on LiMnAs that high-quality single crystals of group-I compounds can be grown by MBE and that the measured optical properties of LiMnAs epilayers are consistent with the predicted semiconducting band structure. Our theoretical and experimental results define a framework for future systematic research of material properties of the broad family of semiconductor I-Mn-V compounds and of the utility of AFM semiconductors in spintronic devices operating at high temperatures.

ACKNOWLEDGMENTS

We thank Petr Jiříček, Zbyněk Šobáň, and Miroslav Maryško for experimental assistance, and we acknowledge support from EU Grants No. FP7-214499 NAMASTE and No. FP7-215368 SemiSpinNet, ERC Advanced Grant No. 268066, Czech Republic Grants No. AV0Z10100520, AV0Z10100521, No. MSM0021620834, No. MSM0021620857, No. KAN400100652, No. LC510, and Preamium Academiae.

---

[1] C. Chappert, A. Fert, and F. N. V. Dau, Nat. Mater. **6**, 813 (2007).

[2] *Spintronics*, Vol. 82 of *Semiconductors and Semimetals*, edited by T. Dietl, D. D. Awschalom, M. Kaminska, and H. Ohmo (Elsevier, Amsterdam, 2008).

[3] J. Wunderlich, T. Jungwirth, B. Kaestner, A. C. Irvine, K. Y. Wang, N. Stone, U. Rana, A. D. Giddings, A. B. Shick, C. T. Foxon, R. P. Campion, D. A. Williams, and B. L. Gallagher, Phys. Rev. Lett. **97**, 077201 (2006).

[4] L. Gao, X. Jiang, S.-H. Yang, J. D. Burton, E. Y. Tsymbal, and S. S. P. Parkin, Phys. Rev. Lett. **99**, 226602 (2007).

[5] B. G. Park, J. Wunderlich, D. A. Williams, S. J. Joo, K. Y. Jung, K. H. Shin, K. Olejník, A. B. Shick, and T. Jungwirth, Phys. Rev. Lett. **100**, 087204 (2008).

[6] A. Bernand-Mantel, P. Seneor, K. Bouzehouane, S. Fusil, C. Deranlot, F. Petroff, and A. Fert, Nat. Phys. **5**, 920 (2009).

[7] A. B. Shick, S. Khmelevskyi, O. N. Mryasov, J. Wunderlich, and T. Jungwirth, Phys. Rev. B **81**, 212409 (2010).

[8] B. G. Park, J. Wunderlich, X. Marti, V. Holy, Y. Kurosaki, M. Yamada, H. Yamamoto, A. Nishide, J. Hayakawa, H. Takahashi, A. B. Shick, and T. Jungwirth, e-print arXiv:1011.3188.

[9] W. A. Harrison, *Electronic Structure and the Properties of Solids* (Freeman, San Francisco, 1980).

[10] E. Zintl and G. Brauer, Z. Phys. Chem. B **20**, 245 (1933).

[11] K. Kuriyama, T. Kato, and K. Kawada, Phys. Rev. B **49**, 11452 (1994).

[12] W. Bronger, P. Müller, R. Höppner, and H. U. Schuster, Z. Anorg. Allg. Chem. **539**, 175 (1986).

[13] R. Muller, M. Kuckel, H. U. Schuster, P. Muller, and W. Bronger, J. Alloys Compd. **176**, 167 (1991).

[14] F. Schucht, A. Dascoulidou, R. Muller, W. Jung, H. U. Schuster, W. Bronger, and P. Muller, Z. Anorg. Allg. Chem. **625**, 31 (1999).

[15] S. Khmelevskyi and P. Mohn, Appl. Phys. Lett. **93**, 162503 (2008).

[16] A. Scholl, M. Liberati, E. Arenholz, H. Ohldag, and J. Stöhr, Phys. Rev. Lett. **92**, 247201 (2004).